



AMTD

7, 1–31, 2014

This discussion paper is/has been under review for the journal Atmospheric Measurement Techniques (AMT). Please refer to the corresponding final paper in AMT if available.

Updated SAO OMI formaldehyde retrieval

G. González Abad¹, X. Liu¹, K. Chance¹, H. Wang¹, T. P. Kurosu², and R. Suleiman¹

¹Harvard-Smithsonian Center for Astrophysics, Cambridge, MA, USA

²Jet Propulsion Laboratory, Pasadena, CA, USA

Received: 29 November 2013 – Accepted: 6 December 2013 – Published: 7 January 2014

Correspondence to: G. González Abad (ggonzalezabad@cfa.harvard.edu)

Published by Copernicus Publications on behalf of the European Geosciences Union.

Discussion Paper | Discussion Paper

SAO OMI H₂CO retrieval

G. González Abad et al.

Title Page

Abstract

Introduction

Conclusions

References

Tables

Figures

◀

▶

◀

▶

Back

Close

Full Screen / Esc

Printer-friendly Version

Interactive Discussion



Abstract

We present and discuss the Smithsonian Astrophysical Observatory (SAO) formaldehyde (H_2CO) retrieval algorithm for the Ozone Monitoring Instrument (OMI) which is the operational retrieval for NASA OMI H_2CO . The version of the algorithm described here includes relevant changes with respect to the operational one, including differences in the reference spectra for H_2CO , the fit of $\text{O}_2\text{-O}_2$ collisional complex, updates in the high resolution solar reference spectrum, the use of a model reference sector over the remote Pacific Ocean to normalize the retrievals, an updated Air Mass Factor (AMF) calculation scheme, and the inclusion of scattering weights and vertical H_2CO profile in the level 2 products. The theoretical basis of the retrieval is discussed in detail. Typical values for retrieved vertical columns are between 4×10^{15} and 4×10^{16} molecules cm^{-2} with typical fitting uncertainties ranging between 40 % and 100 %. In high concentration regions the errors are usually reduced to 30 %. The detection limit is estimated at 3×10^{15} molecules cm^{-2} . These updated retrievals are compared with previous ones.

15 1 Introduction

H_2CO is one of the most abundant hydrocarbons in the troposphere and a key constituent, despite its short lifetime of 1.5 h from photolysis and oxidation by the hydroxyl radical (OH). Background levels of H_2CO (concentrations below 1 ppbv) are sustained by the oxidation of methane, but over continental regions the oxidation of short-lived non-methane volatile organic compounds (NMVOCs) from anthropogenic, biogenic and pyrogenic origins and direct emissions from fires and industrial activities can produce enhanced concentrations of H_2CO within the boundary layer of over 5 ppbv (Houweling et al., 1998; Kanakidou et al., 2005; Lowe and Schmidt, 1983; Parrish et al., 2012). Given its short lifetime, measurements from satellites with enough spatial and temporal resolution can use H_2CO as a proxy for NMVOCs emissions and

AMTD

7, 1–31, 2014

SAO OMI H_2CO retrieval

G. González Abad et al.

[Title Page](#)

[Abstract](#)

[Introduction](#)

[Conclusions](#)

[References](#)

[Tables](#)

[Figures](#)

[◀](#)

[▶](#)

[Back](#)

[Close](#)

[Full Screen / Esc](#)

[Printer-friendly Version](#)

[Interactive Discussion](#)



SAO OMI H₂CO retrieval

G. González Abad et al.

[Title Page](#)[Abstract](#)[Introduction](#)[Conclusions](#)[References](#)[Tables](#)[Figures](#)[|◀](#)[▶|](#)[◀](#)[▶](#)[Back](#)[Close](#)[Full Screen / Esc](#)[Printer-friendly Version](#)[Interactive Discussion](#)

detail. This algorithm is used at SAO, with the necessary adjustments, for the retrieval of other trace gases from OMI and other UV/Vis spectrometers.

This paper first focuses on explaining the column retrievals by describing the OMI instrument characteristics, the spectral fitting, the Slant Column Density (SCD) to Vertical Column Density (VCD) conversion, and the reference sector normalization. It then compares previous SAO H₂CO retrievals with these new ones and, finally, summarizes this study.

2 SAO OMI H₂CO observations

2.1 The OMI instrument

- 10 OMI (Levelt et al., 2006) was launched on July 15, 2004 on board the NASA's Earth Observing System (EOS) Aura platform into a Sun-synchronous polar orbit with an average altitude of 705 km and a period of 99 minutes, giving 14.7 orbits per day. The equator crossing time is 13:42 ETC in the ascending node. OMI measures UV/Visible (UV/Vis) solar back scattered radiation using 2-dimensional CCDs from 270 nm to 15 500 nm in 3 channels: UV-1 from 264 nm to 311 nm, UV-2 from 307 nm to 383 nm, and Vis from 349 nm to 504 nm, with spectral resolutions of 0.63, 0.42 and 0.63 nm, respectively. We use UV-2 for H₂CO retrievals. In nominal operation mode, the information in the across-track direction is binned by a factor of 8, resulting in 60 binned ground pixels in the UV-2 channel. OMI has a cross-track field of view of 115° resulting 20 in a swath of 2600 km, with pixel size between 13 × 24 km² at nadir to 26 × 135 km² at the swath edges, providing daily global coverage.

2.2 SAO OMI H₂CO retrieval

We retrieve VCDs of H₂CO using a two-step approach. First, we spectrally fit OMI radiances to retrieve SCDs using the Basic Optical Differential Spectroscopy (BOAS)

AMTD

7, 1–31, 2014

SAO OMI H₂CO retrieval

G. González Abad et al.

[Title Page](#)

[Abstract](#)

[Introduction](#)

[Conclusions](#)

[References](#)

[Tables](#)

[Figures](#)

◀

▶

◀

▶

[Back](#)

[Close](#)

[Full Screen / Esc](#)

[Printer-friendly Version](#)

[Interactive Discussion](#)



[Title Page](#)[Abstract](#)[Introduction](#)[Conclusions](#)[References](#)[Tables](#)[Figures](#)[|◀](#)[▶|](#)[◀](#)[▶](#)[Back](#)[Close](#)[Full Screen / Esc](#)[Printer-friendly Version](#)[Interactive Discussion](#)

method (Chance, 1998). Second, we convert the SCDs to VCDs using Air Mass Factors (AMFs) calculated offline with a radiative transfer model. Finally, we apply post processing corrections based on a reference sector over the remote Pacific Ocean (Khokhar et al., 2005).

5 2.2.1 Spectral fitting

SCDs of H₂CO are determined by direct fitting of OMI radiances (Chance, 1998). First, irradiances and radiance wavelengths are calibrated using cross-correlation with a high resolution solar spectrum (Caspar and Chance, 1997). We use the high resolution solar spectrum recently published by Chance and Kurucz (2010). Two variables may be fitted 10 in the wavelength calibration, spectral shift and squeeze. As they are highly correlated except for very wide fitting regions, we only fit the spectral shift. Wavelength calibrated radiances are fitted to model spectra beginning with radiances from the remote Pacific Ocean substituting for the daily solar irradiance, and including molecular absorption from O₃ (Malicet et al., 1995), NO₂ (Vandaele et al., 1998), BrO (Wilmouth et al., 1999), 15 the O₂-O₂ collision complex (Thalman and Volkamer, 2013), and H₂CO (Chance and Orphal, 2011), all convolved with the OMI slit function measured prior to launch (Dirksen et al., 2006), an effective albedo, the molecular Ring correction (Chance and Spurr, 1997), a correction accounting for the aliasing introduced from spectral undersampling (Chance, 1998; Chance et al., 2005), which is calculated online, the common mode 20 spectrum obtained by averaging the fitting residuals, also calculated online for each orbit, and two low order closure polynomials that help to account for low frequency features of the measured radiance in the fitting window (Eq. 1).

$$I = \left[\left(aI_0 + \sum_i \alpha_i X_i \right) e^{-\sum_j \alpha_j X_j} + \sum_k \alpha_k X_k \right] \sum_n \alpha_n X_n + \sum_m \alpha_m X_m \quad (1)$$

25 In Eq. (1), a is the albedo, I_0 is the solar irradiance, $\alpha_i X_i$ are terms added before the trace gas contributions, including the Ring spectrum and the undersampling correction,

$\alpha_j X_j$ are the Beer–Lambert law contributions from the trace gases, $\alpha_k X_k$ are the terms added afterwards, including the common mode spectrum, and $\alpha_n X_n$ and $\alpha_m X_m$ are the scaling and baseline closure polynomials.

Instead of using the traditional solar irradiance as I_0 in Eq. (1), we use radiances over the remote Pacific Ocean obtained from an orbit as close to 165° W as possible, measured within 24 h of the orbit to be processed, to build a radiance reference by averaging the radiance spectra over the Pacific between 30° S and 30° N. Then we use this radiance reference as I_0 . Due to the weak absorption of H₂CO, the use of the radiance reference over the Pacific helps to address some instrument issues observed in previous versions of the H₂CO retrieval, including the well-known striping problems of OMI (Veihelmann and Kleipool, 2006). The characteristics of the spectral fit, reference spectra, closure polynomials, and online computed corrections are summarized in Table 1. The SCD that minimizes the cost function χ^2 calculated from the difference between the measured and modeled radiance is retrieved using a non-linear least square inversion method implemented in the ELSUNC software (Lindström and Wedin, 1988). Compared to the Differential Optical Absorption Spectroscopy (DOAS) method, we do not divide radiance by irradiance, take logarithms, apply smoothing, or apply high-pass filtering during our spectral analysis.

We use a fitting window from 328.5 nm to 356.5 nm, similar to other windows reported in the literature for GOME, GOME-2 and SCIAMACHY (De Smedt et al., 2008, 2012). It is a minor change compared with our previous fitting window, 327.5 nm to 356.5 nm, but its use helps to keep the fitting stable over time, minimizing the effects of instrument degradation. Figure 1 shows the residual and the results of the fitting for three pixels of orbit 11118 (17 August 2006) over South America. The thick black line is the fitted H₂CO optical depth and the thin red line is the fitted H₂CO optical depth plus the residual, shown here to provide an idea of the fitting quality. Typical values for the retrieved H₂CO SCDs are in the range from 4×10^{15} to 6×10^{16} molecules cm⁻². Uncertainties range from 6×10^{15} molecules cm⁻² (~30 %) for pixels with high concentrations (above 2×10^{16} molecules cm⁻²) to 100 % or larger for pixels with low concentrations. Fitting

[Title Page](#)[Abstract](#)[Introduction](#)[Conclusions](#)[References](#)[Tables](#)[Figures](#)[|◀](#)[▶|](#)[◀](#)[▶](#)[Back](#)[Close](#)[Full Screen / Esc](#)[Printer-friendly Version](#)[Interactive Discussion](#)

Root Mean Square (RMS) values are between 0.4×10^{-3} and 2.0×10^{-3} , corresponding to detection limits of $\sim 3 \times 10^{15}$ molecules cm^{-2} .

2.2.2 Vertical column density determination

The second step of our retrieval converts SCDs in to VCDs. The photons reaching OMI are either reflected from the Earth's surface and transmitted or scattered to OMI or directly scattered to OMI without reaching the Earth's surface. The retrieved SCDs depend on the viewing geometry for each pixel (solar zenith angle, viewing zenith angle and relative azimuth angle), the surface albedo and the state of the atmosphere (clouds, trace gases concentrations, temperature, air density, pressure, etc). The SCDs are related to the VCDs by AMFs. The relationship between SCDs and VCDs is

$$\text{VCD} = \text{SCD}/\text{AMF}. \quad (2)$$

To determine AMFs, we follow the approach described in Palmer et al. (2001), summarized by Eq. (3).

$$\text{AMF} = \int_{\text{atm}} w(z, \theta_0, \theta, \varphi, a_s, h_s, C_f, C_h) S(z, \text{lat}, \text{lon}, \text{month}) dz. \quad (3)$$

In this formulation, the scattering weights (w) account for the sensitivity of the satellite measurements to the presence of H_2CO molecules at different altitudes. They are functions of altitude (z), solar zenith angle (θ_0), viewing zenith angle (θ), relative azimuth angle (φ), surface albedo (a_s), terrain height (h_s), effective cloud fraction (C_f) and cloud top altitude (C_h). For an optically thin absorber such as H_2CO , the w s are independent of the column abundance of the species. The shape factor (S), dependent on the location and time of the measurement, represents the normalized vertical profile of the absorbing molecule and provides a priori estimation of the vertical distribution of

[Title Page](#)[Abstract](#)[Introduction](#)[Conclusions](#)[References](#)[Tables](#)[Figures](#)[|◀](#)[▶|](#)[◀](#)[▶](#)[Back](#)[Close](#)[Full Screen / Esc](#)[Printer-friendly Version](#)[Interactive Discussion](#)

H_2CO . The shape factor for a particular location and time is defined in Eq. (4).

$$S(z) = \frac{x_a(z)}{\int_{\text{atm}} x_a(z) dz}. \quad (4)$$

x_a is the a priori vertical profile of H_2CO partial columns. We have calculated vertical profiles using the GEOS-Chem (Bey et al., 2001) chemical transport model (Version v9-01-03), which is driven by Goddard Earth Observing System-5 (GEOS-5) assimilated meteorological data products interpolated onto 47 vertical levels at a spatial resolution of 2° latitude $\times 2.5^\circ$ longitude. We have developed a monthly mean climatology using GEOS-Chem simulations between 11:00 and 13:00 LT in 2007. Figure 2 shows a set of vertical profiles used in the AMF calculation for Orbit number 11118 at different latitudes.

We have calculated the scattering weights using the radiative transfer model VLIDORT version 2.4RT (Spurr, 2006). $w(z)$ usually depends on the wavelength and the viewing geometry. However, for solar zenith angles below 70° , since the ozone absorption is not too strong in the 328.5–356.5 nm fitting window, the variation of $w(z)$ with wavelength is small (less than 5%). Therefore, we have used the scattering weights at only one optimized wavelength, 340 nm. For solar zenith angles above 70° , the ozone absorption becomes large enough to make the assumption of an optically thin atmosphere not valid (we concentrate on $\text{SZA} < 70^\circ$). We have prepared a set of weighting function look-up tables that are parameterized by the surface albedo and the relative azimuth angle, with entries for solar zenith angles (12), viewing zenith angles (8), altitudes (48) and cloud-top/surface pressures (6). These parameters are summarized in Table 2. Clouds are assumed to be opaque Lambertian surfaces at a single cloud top height (C_h) with a cloud albedo (a_c) of 0.8–1.0. Partly cloudy pixels are assumed to be a mixture of clear-sky scene and cloudy scene ($a_c = 0.8$) with an effective cloud fraction of C_f calculated using the independent pixel approximation (Martin et al., 2002). Under this approximation, the scattering weight for an inhomogeneous pixel with a given

[Title Page](#)[Abstract](#)[Introduction](#)[Conclusions](#)[References](#)[Tables](#)[Figures](#)[|◀](#)[▶|](#)[Back](#)[Close](#)[Full Screen / Esc](#)[Printer-friendly Version](#)[Interactive Discussion](#)

viewing geometry becomes

$$w = (1 - \Phi) \cdot w_{\text{clear}}(a_s, h_s) + \Phi \cdot w_{\text{cloud}}(a_c, C_h), \quad (5)$$

where, w_{clear} is the scattering weight for the clear sky part of the pixel, a_s is the surface albedo, h_s is the terrain height, w_{cloud} is the scattering weight of the cloudy part of the pixel, C_h is the cloud top height and Φ is the intensity-weighted cloud fraction or radiative cloud fraction calculated as

$$\Phi = \frac{C_f \cdot I_{\text{cloud}}}{(1 - C_f) \cdot I_{\text{clear}} + C_f \cdot I_{\text{cloud}}}. \quad (6)$$

¹⁰ I_{clear} and I_{cloud} are the radiance intensities for clear-sky and cloudy scenes at the top of the atmosphere. The values of I_{clear} and I_{cloud} are calculated using VLIDORT and stored in a look-up table with the same parameter grid as the weighting function look-up table. The a_s used to evaluate w_{clear} and I_{clear} is obtained from the OMI surface reflectance climatology (Kleipool et al., 2008) while h_s is provided with the OMI level 1B product (OML1BRUG). The description of clouds is consistent with the assumptions used in the cloud retrieval algorithm (Acarreta et al., 2004; Stammes et al., 2008) from which we obtain C_f and C_h distributed in the Aura OMI Cloud Data Product-OMCLDO2. Figure 3 shows the scattering weights for three pixels of Orbit 11118 with low, medium and high effective cloud fractions. Once the scattering weights are calculated, the averaging

¹⁵ kernels (AK) (Rodgers and Connor, 2003) are straightforward to be approximated using the formulation below for DOAS retrievals (Eskes and Boersma, 2003):

²⁰

$$\text{AK}(z) = \frac{w(z)}{\text{AMF}}. \quad (7)$$

²⁵ w_z is calculated as in Eq. (5) and AMFs are described in Eq. (3). Model comparisons with H₂CO VCDs, assimilation of OMI H₂CO products, and validation with H₂CO profiles should make use of the scattering weights and the used H₂CO vertical profiles, so we provide them along with the columns.

[Title Page](#)

[Abstract](#)

[Introduction](#)

[Conclusions](#)

[References](#)

[Tables](#)

[Figures](#)

[|◀](#)

[▶|](#)

[◀](#)

[▶](#)

[Back](#)

[Close](#)

[Full Screen / Esc](#)

[Printer-friendly Version](#)

[Interactive Discussion](#)



[Title Page](#)[Abstract](#)[Introduction](#)[Conclusions](#)[References](#)[Tables](#)[Figures](#)[|◀](#)[▶|](#)[Back](#)[Close](#)[Full Screen / Esc](#)[Printer-friendly Version](#)[Interactive Discussion](#)

The errors associated with AMF calculations are estimated to be around 30 % dominated by H₂CO vertical profiles, surface albedos, cloud parameters and the presence of aerosols in the pixel scene. The AMF uncertainties combined with the estimated errors on the SCDs (30–100 %) result in the uncertainties associated with VCDs between 5 40 % and 105%. A full error analysis for the H₂CO VCDs will be presented in a paper currently being prepared.

2.2.3 Post-processing normalization of retrieved columns

We derive a daily post-processing normalization for the retrieved columns according to the concentrations simulated by GEOS-Chem (Bey et al., 2001) over the remote 10 Pacific, following an approach similar to Khokhar et al. (2005) and De Smedt et al. (2008). In this region, the H₂CO concentrations are assumed to be at the background levels, their only source being CH₄ oxidation.

We define the reference sector as the region in between 140° W and 160° W and 90° N to 90° S. Using 2.0° latitude by 2.5° longitude model results in 2007, we have built 15 a monthly mean climatology of VCDs by longitudinally averaging concentrations for a given latitude and then latitudinally interpolating the results to a grid of 500 points extending from 90° N to 90° S with a resolution of 0.36°. With these climatological values, taking into consideration the viewing geometry and atmospheric conditions of each pixel (i.e. AMF), we correct the effects of the row anomaly and stripping and normalize 20 the retrieved values to the reference sector to remove the artificially increasing background H₂CO values using the following approach.

We calculate a pixel-by-pixel correction (Eq. 8) over the remote Pacific Ocean (radiance reference granule) only using pixels with main quality flag equal to 0. For these pixels the fitting is successful and the retrieved VCD is within two standard deviations 25 of the average VCD for the whole orbit.

$$\text{Correction}(i, j) = \text{OMI}_{\text{Pacific}}(i, j) - (\text{GEOS_Chem}_{\text{ReferenceSector}}(\text{lat}) \times \text{AMF}(i, j)). \quad (8)$$

SAO OMI H₂CO retrieval

G. González Abad et al.

[Title Page](#)[Abstract](#)[Introduction](#)[Conclusions](#)[References](#)[Tables](#)[Figures](#)[|◀](#)[▶|](#)[◀](#)[▶](#)[Back](#)[Close](#)[Full Screen / Esc](#)[Printer-friendly Version](#)[Interactive Discussion](#)

i is the cross track position (longitude) within an OMI orbit, *j* is the line position (latitude), and lat is the latitude at the center of pixel (*i*, *j*) of the orbit.

After working the correction using the radiance reference orbit we assume that the bias between the retrieved columns and the modeled columns over the remote Pacific

Ocean is representative of a longitudinally invariant bias that affects the retrievals everywhere else on the globe. Therefore, we calculate a latitude dependent correction of this bias for each cross track position using the median values of the corrections calculated in Eq. (8) falling within two points of the reference sector latitude grid. Finally we interpolate these values to the corresponding latitude at the center of each pixel for the rest of the orbits.

We attribute this bias mainly to instrumental issues whose effects are weaker than the row anomaly, and to correlations between BrO and H₂CO absorption cross sections, which are especially significant at high latitudes. We calculate the correction for this bias for each one of the radiance reference orbits over the remote Pacific ocean.

We consider this bias correction to be orbit invariant for all the retrievals performed with the same radiance reference (with in 24 h difference). Therefore we apply it to all OMI columns retrieved from different granules over the globe (typically between 7 and 17 granules for each radiance reference). The final corrected columns are calculated as:

$$\text{VCD}_{\text{corrected}}(i, j) = \frac{\text{SCD}(i, j) - \text{Correction}(i, j)}{\text{AMF}(i, j)}. \quad (9)$$

Figure 4 illustrates the GEOS-Chem results used in the calculation of the background levels for August 2007. Figure 5 shows the longitudinally averaged values computed for each month. We consider the month-to-month variation to be representative of the changes in the background values, in comparison to the rapid spatial and temporal variation in concentrations over the continental hotspots. Despite the correction to the pixels affected by the row anomaly, we still recommend using them with extreme caution.

We will assess the reliability of the bias-corrected columns more rigorously over time. Even though the correction helps us to remove unrealistic biases associated with the

[Title Page](#)[Abstract](#)[Introduction](#)[Conclusions](#)[References](#)[Tables](#)[Figures](#)[|◀](#)[▶|](#)[◀](#)[▶](#)[Back](#)[Close](#)[Full Screen / Esc](#)[Printer-friendly Version](#)[Interactive Discussion](#)

instrument and some trace gases correlations, it introduces external a priori information subject to uncertainties and assumes H₂CO over the reference sector does not change from year to year. This situation should be considered when using the reference sector corrected columns. We provide in our data files both the reference sector corrected columns and the non-corrected VCDs.

3 Comparison between previous and current H₂CO SAO product

Three years of data are used to compare the old and new SAO H₂CO products. Years 2006 and 2007, near the beginning of the mission, are representative of a time when the previous SAO product is quite stable, while year 2012 is representative of a time when the previous SAO product is affected by problems, including the row anomaly and increasing background concentrations.

In general, the new product is less noisy, with smaller fitting uncertainties. This can be seen for the particular case of Orbit 43214 (August 2012) in Fig. 6. The decrease in uncertainty is evident with almost all pixels having an absolute uncertainty smaller than that in the older version of the SAO retrieval. There is also significant reduction of unrealistically high SCDs.

The general increase in the retrieved columns in the previous SAO retrieval is so large that it is difficult to use after 2010 (Kim et al., 2011). In the new retrieval, the situation is greatly improved. In Fig. 7 (for Orbit 43214) we have plotted the retrieved VCDs for the old retrieval, the new one and the new one with the reference sector correction applied to show how the situation has improved in our new retrieval. The first panel, top left, gives VCDs retrieved with the old algorithm. Extremely high values (over 2.0×10^{16}) are common over the continents and equatorial ocean areas, while there are areas of negative values at high latitudes.

With the new algorithm without the reference sector correction, top right panel, it is evident that there is significant reduction in the concentrations almost everywhere. However, the contrast between high and low concentration regions increases. The new

retrieval also has fewer pixels with negative values at high latitudes. After we applied the reference sector correction (bottom left panel), the situation further improves. As mentioned earlier, the new retrieval still shows large negative concentrations, but smaller in the new version, at high latitudes due to correlations with BrO. Applying the reference
5 sector correction helps to minimize this effect as well as to reduce the effect of the row anomaly. Finally, we plot the difference between the VCDs retrieved with the old and the new products in the bottom right panel. The concentrations are reduced almost everywhere in the orbit (blue colors). We only see increases in concentrations where the old retrieval is consistently negative. There is huge improvement for pixels affected
10 by the row anomaly in the new retrieval. However, we still caution using pixels affected by the row anomaly until the new retrievals are fully validated.

We now compare level 3 monthly averages to better assess changes in the concentrations and to examine the trends observed in previous retrievals. To compute monthly averages, we only considered pixels with cloud fractions below 40 % and unaffected
15 by the row anomaly. The level 3 data are calculated on a $0.2^\circ \times 0.2^\circ$ grid where values of the OMI pixel are weighted by the area falling with the grid box and by the fitting uncertainty.

We have defined five regions in this study. Background levels over the remote Pacific Ocean (A), Southeast USA (B), the Amazon basin (C), Europe (D) and Southeast Asia (E). The areas used for each of these regions are shown in Fig. 4. We have focused our analysis on 2006, 2007 and 2012. While the old SAO retrieval is stable until the end of 2007, by 2012 it is clearly producing unreasonable columns over the Pacific and an overall increase of the retrieved concentrations worldwide. The selected three years are thus appropriate for comparing the old and the new results.
20

Figure 8 shows the results of the time series comparison. Overall, the new retrieval (red and green lines) is more stable over time. It doesn't show a large increasing trend in the overall concentrations. The background concentrations over the Pacific Ocean remain almost the same for the new retrieval, while the old SAO retrieval exhibits an increase of 0.3×10^{16} molecules cm^{-2} between the end of 2007 and the beginning of
25

SAO OMI H_2CO retrieval

G. González Abad et al.

[Title Page](#)

[Abstract](#)

[Introduction](#)

[Conclusions](#)

[References](#)

[Tables](#)

[Figures](#)

[|◀](#)

[▶|](#)

[◀](#)

[▶](#)

[Back](#)

[Close](#)

[Full Screen / Esc](#)

[Printer-friendly Version](#)

[Interactive Discussion](#)



2012. The other regions have similar seasonality in the old and new retrievals, but the sharp increase in the background levels from 2007 to 2012 for the old retrieval is present, especially in the southeastern USA and Southeast Asia. The retrieved columns in the new version don't show significant jumps. For the new retrieval, the
5 main remaining issue is the too high winter concentrations over Europe. We recommend at present the values for December, January and February over North Europe to be used with caution.

Figure 9 shows the results for the new retrieval without the reference sector correction applied in the middle panels, with the reference sector correction applied in the
10 right panels and the old SAO retrieval in the left panels. These plots are seasonal averages for DJF, MAM, JJA and SON. The reduction in the background values is evident in the new retrieval. Hot spots are more spatially resolved in the new retrieval, e.g., the hot spot over Central America in MAM). The high concentrations over the Mediterranean Sea in JJA are removed. The worst issue with the new retrieval, as mentioned above,
15 is unrealistically high concentrations over Europe during winter months.

4 Conclusions

We have presented and discussed the new SAO OMI H₂CO retrieval especially the
new updates to the operational algorithm. Reference spectroscopy updates, the use of
an improved high resolution solar spectrum, and the different analysis approaches that
20 are introduced to improve accuracy and precision and to fix the instability of the old
SAO retrieval. We have slightly modified the fitting window and used a reference sector
over the remote Pacific Ocean to correct for possible biases and their temporal drift in
the retrieved slant columns.

The columns retrieved by the new SAO OMI H₂CO algorithm show more stability over
time. The increasing trend in concentrations is greatly reduced, as is the noise of the
25 retrieved columns. This new product greatly extends the volume of useful H₂CO data
from OMI beyond 2008 and also provides new data to facilitate its use. The scattering

SAO OMI H₂CO retrieval

G. González Abad et al.

[Title Page](#)

[Abstract](#)

[Introduction](#)

[Conclusions](#)

[References](#)

[Tables](#)

[Figures](#)

[|◀](#)

[▶|](#)

[◀](#)

[▶](#)

[Back](#)

[Close](#)

[Full Screen / Esc](#)

[Printer-friendly Version](#)

[Interactive Discussion](#)



SAO OMI H₂CO retrieval

G. González Abad et al.

[Title Page](#)[Abstract](#)[Introduction](#)[Conclusions](#)[References](#)[Tables](#)[Figures](#)[|◀](#)[▶|](#)[◀](#)[▶](#)[Back](#)[Close](#)[Full Screen / Esc](#)[Printer-friendly Version](#)[Interactive Discussion](#)

weights used in the SCD to VCD inversion and the associated H₂CO vertical profiles are now included in the L2 data files for use in model comparisons. We now include a quality flag in our product for problems caused by instrument row anomaly. As a general rule, we recommend users not to use pixels affected by the row anomaly.

We have also described in detail the theoretical basis of the algorithms used at SAO for retrieval of trace gas gases from OMI and other UV/Vis spectrometers.

The new SAO H₂CO retrieval has several advantages over the old operational SAO-NASA retrieval. The noise is reduced, the fitting uncertainties are smaller, the increasing trends over time are mitigated, and new data fields, including scattering weights and row anomaly flags are available.

A detailed error analysis is in preparation. We are also working on further validation of our new product.

Acknowledgements. This study is supported by NASA Atmospheric Composition Program/Aura Science Team (NNX11AE58G) and the Smithsonian Institution. The Dutch-Finnish OMI instrument is part of the NASA EOS Aura satellite payload. The OMI Project is managed by NIVR and KNMI in the Netherlands. We acknowledge the OMI International Science Team for providing OMI data used in this study.

References

Acarreta, J. R., De Haan, J. F., and Stammes, P.: Cloud pressure retrieval using the O₂-O₂ absorption band at 477 nm, *J. Geophys. Res.-Atmos.*, 109, D05204, doi:10.1029/2003JD003915, 2004. 9

Barkley, M. P., Palmer, P. I., Kuhn, U., Kesselmeier, J., Chance, K., Kurosu, T. P., Martin, R. V., Helmig, D., and Guenther, A.: Net ecosystem fluxes of isoprene over tropical South America inferred from Global Ozone Monitoring Experiment (GOME) observations of HCHO columns, *J. Geophys. Res.-Atmos.*, 113, D20304, doi:10.1029/2008JD009863, 2008. 3

Bey, I., Jacob, D. J., Yantosca, R. M., Logan, J. A., Field, B. D., Fiore, A. M., Li, Q., Liu, H. Y., Mickley, L. J., and Schultz, M. G.: Global modeling of tropospheric chemistry with assimil-

lated meteorology: model description and evaluation, *J. Geophys. Res.-Atmos.*, 106, 23073–23095, doi:10.1029/2001JD000807, 2001. 8, 10

Caspar, C. and Chance, K.: GOME wavelength calibration using solar and atmospheric spectra, in: Third ERS Symposium on Space at the Service of Our Environment, edited by: Guyenne, T.-D. and Danesy, D., vol. 414 of *ESA Special Publication*, 609, 1997. 5

Chance, K.: Analysis of BrO measurements from the Global Ozone Monitoring Experiment, *Geophys. Res. Lett.*, 25, 3335–3338, doi:10.1029/98GL52359, 1998. 5

Chance, K. and Kurucz, R.: An improved high-resolution solar reference spectrum for earth's atmosphere measurements in the ultraviolet, visible, and near infrared, *J. Quant. Spectrosc. Ra.*, 111, 1289–1295, doi:10.1016/j.jqsrt.2010.01.036, 2010. 5, 21

Chance, K. and Orphal, J.: Revised ultraviolet absorption cross sections of H₂CO for the HITRAN database, *J. Quant. Spectrosc. Ra.*, 112, 1509–1510, doi:10.1016/j.jqsrt.2011.02.002, 2011. 5, 21

Chance, K. V. and Spurr, R. J. D.: Ring effect studies: Rayleigh scattering, including molecular parameters for rotational Raman scattering, and the Fraunhofer spectrum, *Appl. Optics*, 36, 5224–5230, doi:10.1364/AO.36.005224, 1997. 5, 21

Chance, K., Palmer, P. I., Spurr, R. J. D., Martin, R. V., Kurosu, T. P., and Jacob, D. J.: Satellite observations of formaldehyde over North America from GOME, *Geophys. Res. Lett.*, 27, 3461–3464, doi:10.1029/2000GL011857, 2000. 3

Chance, K., Kurosu, T. P., and Sioris, C. E.: Undersampling correction for array detector-based satellite spectrometers, *Appl. Optics*, 44, 1296–1304, doi:10.1364/AO.44.001296, 2005. 5, 21

De Smedt, I., Müller, J.-F., Stavrakou, T., van der A, R., Eskes, H., and Van Roozendael, M.: Twelve years of global observations of formaldehyde in the troposphere using GOME and SCIAMACHY sensors, *Atmos. Chem. Phys.*, 8, 4947–4963, doi:10.5194/acp-8-4947-2008, 2008. 3, 6, 10

De Smedt, I., Van Roozendael, M., Stavrakou, T., Müller, J.-F., Lerot, C., Theys, N., Valks, P., Hao, N., and van der A, R.: Improved retrieval of global tropospheric formaldehyde columns from GOME-2/MetOp-A addressing noise reduction and instrumental degradation issues, *Atmos. Meas. Tech.*, 5, 2933–2949, doi:10.5194/amt-5-2933-2012, 2012. 3, 6

Dirksen, R., Dobber, M., Voors, R., and Levelt, P.: Prelaunch characterization of the Ozone Monitoring Instrument transfer function in the spectral domain, *Appl. Optics*, 45, 3972–3981, doi:10.1364/AO.45.003972, 2006. 5, 21

[Title Page](#)

[Abstract](#)

[Introduction](#)

[Conclusions](#)

[References](#)

[Tables](#)

[Figures](#)

◀

▶

◀

▶

[Back](#)

[Close](#)

[Full Screen / Esc](#)

[Printer-friendly Version](#)

[Interactive Discussion](#)



- Dufour, G., Szopa, S., Barkley, M. P., Boone, C. D., Perrin, A., Palmer, P. I., and Bernath, P. F.: Global upper-tropospheric formaldehyde: seasonal cycles observed by the ACE-FTS satellite instrument, *Atmos. Chem. Phys.*, 9, 3893–3910, doi:10.5194/acp-9-3893-2009, 2009. 3
- Eskes, H. J. and Boersma, K. F.: Averaging kernels for DOAS total-column satellite retrievals, *Atmos. Chem. Phys.*, 3, 1285–1291, doi:10.5194/acp-3-1285-2003, 2003. 9
- Fu, T.-M., Jacob, D. J., Palmer, P. I., Chance, K., Wang, Y. X., Barletta, B., Blake, D. R., Stanton, J. C., and Pilling, M. J.: Space-based formaldehyde measurements as constraints on volatile organic compound emissions in east and south Asia and implications for ozone, *J. Geophys. Res.-Atmos.*, 112, D06312, doi:10.1029/2006JD007853, 2007. 3
- Heckel, A., Richter, A., Tarsu, T., Wittrock, F., Hak, C., Pundt, I., Junkermann, W., and Burrows, J. P.: MAX-DOAS measurements of formaldehyde in the Po-Valley, *Atmos. Chem. Phys.*, 5, 909–918, doi:10.5194/acp-5-909-2005, 2005. 3
- Houweling, S., Dentener, F., and Lelieveld, J.: The impact of nonmethane hydrocarbon compounds on tropospheric photochemistry, *J. Geophys. Res.-Atmos.*, 103, 10673–10696, doi:10.1029/97JD03582, 1998. 2
- Jones, N. B., Riedel, K., Allan, W., Wood, S., Palmer, P. I., Chance, K., and Notholt, J.: Long-term tropospheric formaldehyde concentrations deduced from ground-based fourier transform solar infrared measurements, *Atmos. Chem. Phys.*, 9, 7131–7142, doi:10.5194/acp-9-7131-2009, 2009. 3
- Kanakidou, M., Seinfeld, J. H., Pandis, S. N., Barnes, I., Dentener, F. J., Facchini, M. C., Van Dingenen, R., Ervens, B., Nenes, A., Nielsen, C. J., Swietlicki, E., Putaud, J. P., Balkanski, Y., Fuzzi, S., Horth, J., Moortgat, G. K., Winterhalter, R., Myhre, C. E. L., Tsigaridis, K., Vignati, E., Stephanou, E. G., and Wilson, J.: Organic aerosol and global climate modelling: a review, *Atmos. Chem. Phys.*, 5, 1053–1123, doi:10.5194/acp-5-1053-2005, 2005. 2
- Khokhar, M., Frankenberg, C., Rozendaal, M. V., Beirle, S., Kuhl, S., Richter, A., Platt, U., and Wagner, T.: Satellite observations of atmospheric SO₂ from volcanic eruptions during the time-period of 19962002, *Adv. Space Res.*, 36, 879–887, doi:10.1016/j.asr.2005.04.114, 2005. 5, 10
- Kim, J. H., Kim, S. M., Baek, K. H., Wang, L., Kurosu, T., De Smedt, I., Chance, K., and Newchurch, M. J.: Evaluation of satellite-derived HCHO using statistical methods, *Atmos. Chem. Phys. Discuss.*, 11, 8003–8025, doi:10.5194/acpd-11-8003-2011, 2011. 3, 12

AMTD

7, 1–31, 2014

SAO OMI H₂CO retrieval

G. González Abad et al.

[Title Page](#)

[Abstract](#)

[Introduction](#)

[Conclusions](#)

[References](#)

[Tables](#)

[Figures](#)

◀

▶

[Back](#)

[Close](#)

[Full Screen / Esc](#)

[Printer-friendly Version](#)

[Interactive Discussion](#)



SAO OMI H₂CO retrieval

G. González Abad et al.

[Title Page](#)[Abstract](#)[Introduction](#)[Conclusions](#)[References](#)[Tables](#)[Figures](#)[◀](#)[▶](#)[◀](#)[▶](#)[Back](#)[Close](#)[Full Screen / Esc](#)[Printer-friendly Version](#)[Interactive Discussion](#)

Kleipool, Q. L., Dobber, M. R., de Haan, J. F., and Levelt, P. F.: Earth surface reflectance climatology from 3 years of OMI data, *J. Geophys. Res.-Atmos.*, 113, D18, doi:10.1029/2008JD010290, 2008. 9

Kurosu, T. P., Chance, K., and Sioris, C. E.: Preliminary results for HCHO and BrO from the EOS-Aura Ozone Monitoring Instrument, *Proc. SPIE*, 5652, 116–123, doi:10.1117/12.578606, 2004. 3

Levelt, P. F., van den Oord, G. H. J., Dobber, M. R., Mälkki, A., Visser, H., de Vries, J., Stammes, P., Lundell, J. O. V., and Saari, H.: The ozone monitoring instrument, *IEEE T. Geosci. Remote*, 44, 1093–1101, doi:10.1109/TGRS.2006.872333, 2006. 4

Lindström, P. and Wedin, P.-A.: Methods and software for nonlinear least squares problems, Technical report UMINF-133.87, Inst. of Information Processing, University of Umeå, Umeå, Sweden, 1988. 6

Lowe, D. C. and Schmidt, U.: Formaldehyde (HCHO) measurements in the nonurban atmosphere, *J. Geophys. Res.-Oceans*, 88, 10844–10858, doi:10.1029/JC088iC15p10844, 1983. 2

Malicet, J., Daumont, D., Charbonnier, J., Parisse, C., Chakir, A., and Brion, J.: Ozone UV spectroscopy, II. Absorption cross-sections and temperature dependence, *J. Atmos. Chem.*, 21, 263–273, doi:10.1007/BF00696758, 1995. 5, 21

Marais, E. A., Jacob, D. J., Kurosu, T. P., Chance, K., Murphy, J. G., Reeves, C., Mills, G., Casadio, S., Millet, D. B., Barkley, M. P., Paulot, F., and Mao, J.: Isoprene emissions in Africa inferred from OMI observations of formaldehyde columns, *Atmos. Chem. Phys.*, 12, 6219–6235, doi:10.5194/acp-12-6219-2012, 2012. 3

Martin, R. V., Chance, K., Jacob, D. J., Kurosu, T. P., Spurr, R. J. D., Bucsela, E., Gleason, J. F., Palmer, P. I., Bey, I., Fiore, A. M., Li, Q., Yantosca, R. M., and Koelemeijer, R. B. A.: An improved retrieval of tropospheric nitrogen dioxide from GOME, *J. Geophys. Res.-Atmos.*, 107, ACH 9–1–ACH 9–21, doi:10.1029/2001JD001027, 2002. 8

Palmer, P. I., Jacob, D. J., Chance, K., Martin, R. V., Spurr, R. J. D., Kurosu, T. P., Bey, I., Yantosca, R., Fiore, A., and Li, Q.: Air mass factor formulation for spectroscopic measurements from satellites: Application to formaldehyde retrievals from the Global Ozone Monitoring Experiment, *J. Geophys. Res.-Atmos.*, 106, 14539–14550, doi:10.1029/2000JD900772, 2001. 3, 7

Parrish, D. D., Ryerson, T. B., Mellqvist, J., Johansson, J., Fried, A., Richter, D., Walega, J. G., Washenfelder, R. A., de Gouw, J. A., Peischl, J., Aikin, K. C., McKeen, S. A., Frost, G. J.,

SAO OMI H₂CO retrieval

G. González Abad et al.

[Title Page](#)[Abstract](#)[Introduction](#)[Conclusions](#)[References](#)[Tables](#)[Figures](#)[|◀](#)[▶|](#)[◀](#)[▶](#)[Back](#)[Close](#)[Full Screen / Esc](#)[Printer-friendly Version](#)[Interactive Discussion](#)

Thalman, R. and Volkamer, R.: Temperature dependent absorption cross-sections of O₂-O₂ collision pairs between 340 and 630 nm and at atmospherically relevant pressure, *Phys. Chem. Chem. Phys.*, 15, 15371–15381, doi:10.1039/C3CP50968K, 2013. 5, 21

Vandaele, A., Hermans, C., Simon, P., Carleer, M., Colin, R., Fally, S., Mérienne, M., Je-
5 nouvrier, A., and Coquart, B.: Measurements of the NO₂ absorption cross-section from
42 000cm⁻¹ to 10 000cm⁻¹ (238–1000nm) at 220 K and 294 K, *J. Quant. Spectrosc. Ra.*,
59, 171–184, doi:10.1016/S0022-4073(97)00168-4, 1998. 5, 21

Veihelmann, B. and Kleipool, Q.: Reducing Along-Track Stripes in OMI-Level 2 Products,
Technical report TN-OMIE-KNMI-785, KNMI, available at: http://disc.sci.gsfc.nasa.gov/Aura/data holdings/OMI/documents/v003/RD08_TN785_i1 Reducing_AlongTrack_Stripes.pdf(last access: 16 March 2006), 2006. 6

Vigouroux, C., Hendrick, F., Stavrakou, T., Dils, B., De Smedt, I., Hermans, C., Merlaud, A.,
Scolas, F., Senten, C., Vanhaelewijn, G., Fally, S., Carleer, M., Metzger, J.-M., Müller, J.-F.,
Van Roozendael, M., and De Mazière, M.: Ground-based FTIR and MAX-DOAS observations
15 of formaldehyde at Réunion Island and comparisons with satellite and model data, *Atmos. Chem. Phys.*, 9, 9523–9544, doi:10.5194/acp-9-9523-2009, 2009. 3

Wagner, T., Beirle, S., Brauers, T., Deutschmann, T., Frieß, U., Hak, C., Halla, J. D., Heue, K. P.,
Junkermann, W., Li, X., Platt, U., and Pundt-Gruber, I.: Inversion of tropospheric profiles of
aerosol extinction and HCHO and NO₂ mixing ratios from MAX-DOAS observations in Milano
20 during the summer of 2003 and comparison with independent data sets, *Atmos. Meas. Tech.*,
4, 2685–2715, doi:10.5194/amt-4-2685-2011, 2011. 3

Wilsmuth, D. M., Hanisco, T. F., Donahue, N. M., and Anderson, J. G.: Fourier Transform Ul-
traviolet Spectroscopy of the A²Π_{3/2} ← X²Π_{3/2} Transition of BrO[†], *J. Phys. Chem. A*, 103,
8935–8945, doi:10.1021/jp991651o, 1999. 5, 21

25 Wittrock, F., Richter, A., Oetjen, H., Burrows, J. P., Kanakidou, M., Myriokefalitakis, S., Volk-
ammer, R., Beirle, S., Platt, U., and Wagner, T.: Simultaneous global observations of glyoxal and
formaldehyde from space, *Geophys. Res. Lett.*, 33, L16804, doi:10.1029/2006GL026310,
2006. 3

AMTD

7, 1–31, 2014

SAO OMI H₂CO
retrieval

G. González Abad et al.

Title Page

Abstract

Introduction

Conclusions

References

Tables

Figures

◀

▶

Back

Close

Full Screen / Esc

Printer-friendly Version

Interactive Discussion



SAO OMI H₂CO retrieval

G. González Abad et al.

Table 1. Fitting window and parameters for deriving H₂CO Slant Column Density.

Fitting window	328.5–356.5 nm
Radiance Reference Spectrum	Computed online over the remote Pacific ocean between 30° N and 30° S
Baseline polynomial	3rd order
Scaling polynomial	3rd order
Instrument slit function	Hyper-parameterization of pre-flight measurements (Dirksen et al., 2006)
Solar Reference Spectrum	Chance and Kurucz (2010)
H ₂ CO cross-sections	Chance and Orphal (2011), 300K
O ₃ cross-sections	Malicet et al. (1995), 228K & 295K
NO ₂ cross-sections	Vandaele et al. (1998), 220K
BrO cross-sections	Wilmouth et al. (1999), 228K
O ₂ -O ₂ collision complex cross-sections	Thalman and Volkamer (2013), 293K
Molecular Ring cross sections	(Chance and Spurr, 1997)
Undersampling correction	Computed online (Chance et al., 2005)
Residual common mode spectrum	Computed online between 30° N and 30° S

[Title Page](#)[Abstract](#)[Introduction](#)[Conclusions](#)[References](#)[Tables](#)[Figures](#)[|◀](#)[▶|](#)[◀](#)[▶](#)[Back](#)[Close](#)[Full Screen / Esc](#)[Printer-friendly Version](#)[Interactive Discussion](#)

Table 2. Parameters of the weighting function look up table.

Parameter	Grid values
Solar zenith angle	0, 15, 30, 45, 60, 70, 77, 81, 84, 86, 88, 89 [°]
Viewing zenith angle	0, 15, 30, 45, 60, 70, 75, 80 [°]
Altitude	0.06, 0.19, 0.32, 0.45, 0.59, 0.73, 0.86, 1.00, 1.15, 1.29, 1.44, 1.58, 1.76, 1.99, 2.25, 2.52, 2.79, 3.08, 3.44, 3.90, 4.38, 4.88, 5.42, 5.98, 6.59, 7.24, 7.95, 8.86, 9.96, 11.04, 12.11, 13.15, 14.19, 15.22, 16.24, 17.26, 18.81, 20.93, 23.12, 25.42, 29.16, 34.65, 40.93, 48.04, 55.86, 64.16, 74.49, 80.79 [km]
Cloud-top/surface pressure	1.00, 0.83, 0.63, 0.52, 0.37, 0.24 [atm]

[Title Page](#)[Abstract](#)[Introduction](#)[Conclusions](#)[References](#)[Tables](#)[Figures](#)[|◀](#)[▶|](#)[Back](#)[Close](#)[Full Screen / Esc](#)[Printer-friendly Version](#)[Interactive Discussion](#)

SAO OMI H₂CO retrieval

G. González Abad et al.

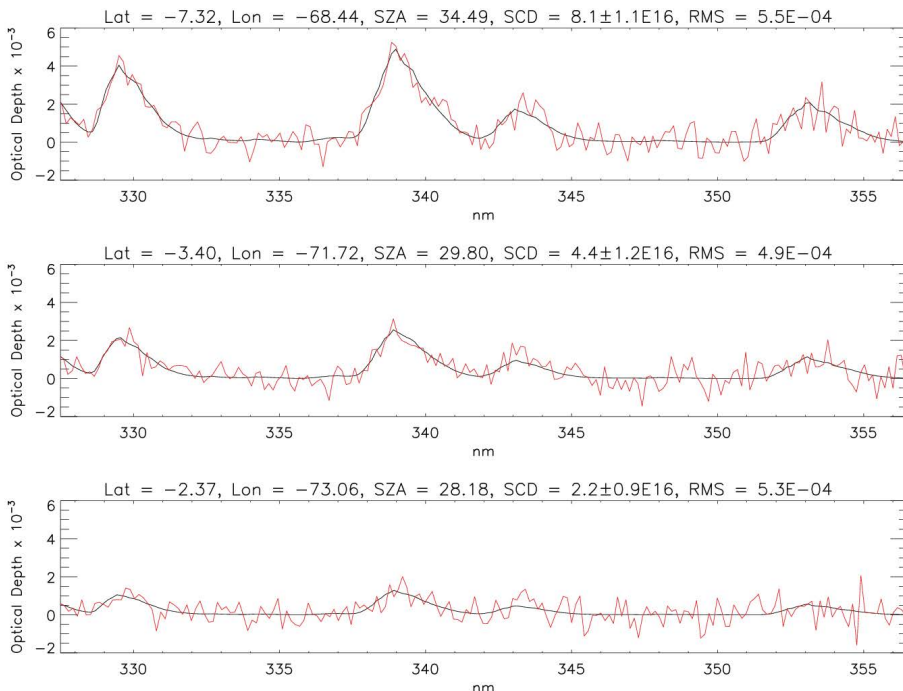


Fig. 1. Fitting of H₂CO in OMI Orbit 11118 (17 August 2006 overpass South America) for high (top), medium (middle), and low (bottom) amounts. The black line is the fitted H₂CO optical depth and the red line is the fitted H₂CO optical depth plus the fitting residuals.

Title Page

Abstract

Introduction

Conclusions

References

Tables

Figures

|◀

▶|

◀

▶

Back

Close

Full Screen / Esc

Printer-friendly Version

Interactive Discussion



SAO OMI H₂CO retrieval

G. González Abad et al.

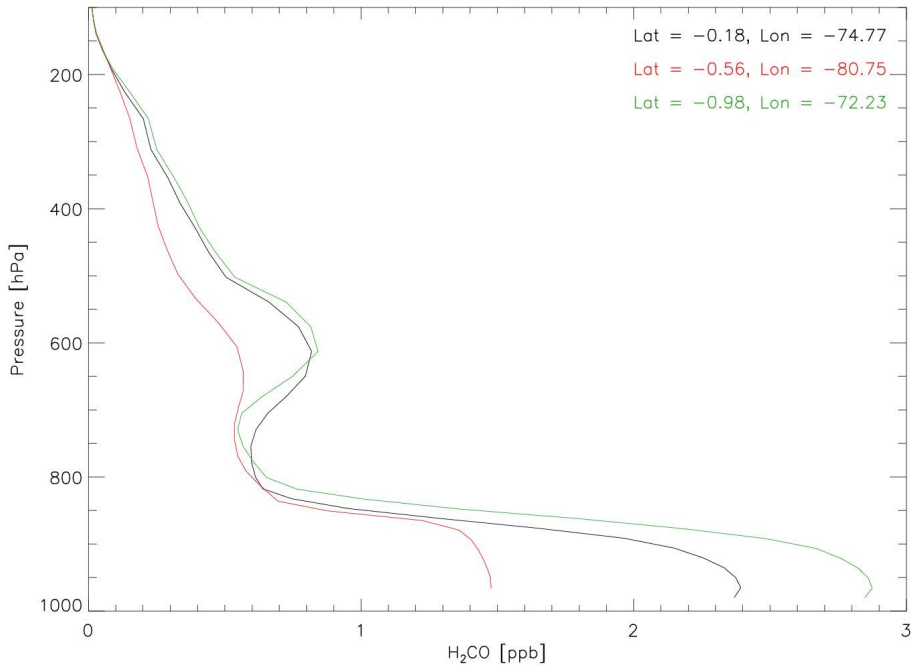


Fig. 2. Three a priori H₂CO profiles used in the air mass factor calculations for Orbit 11118.

[Title Page](#)[Abstract](#)[Introduction](#)[Conclusions](#)[References](#)[Tables](#)[Figures](#)[|◀](#)[▶|](#)[◀](#)[▶](#)[Back](#)[Close](#)[Full Screen / Esc](#)[Printer-friendly Version](#)[Interactive Discussion](#)

SAO OMI H₂CO
retrieval

G. González Abad et al.

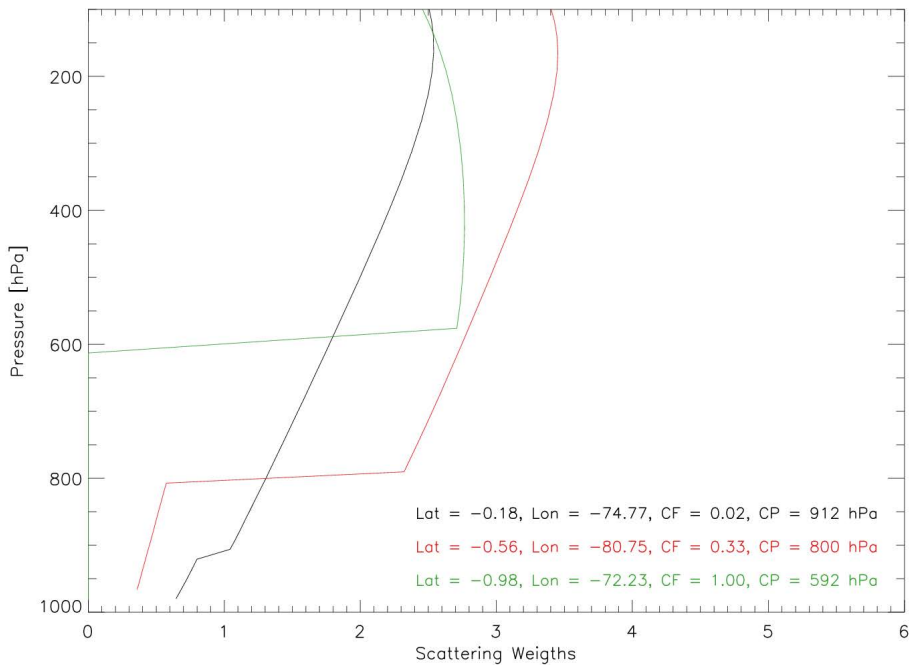


Fig. 3. Example of calculated scattering weights for 3 pixels with different cloud fractions corresponding to the profiles plotted in Fig. 2. For cloud fractions equal to 1 the scattering weights below the cloud top pressure become 0 (green line) while for other values there is a contribution below the cloud in the air mass factor calculation (red and black lines) proportional to the radiative cloud fraction.

- [Title Page](#)
- [Abstract](#) [Introduction](#)
- [Conclusions](#) [References](#)
- [Tables](#) [Figures](#)
- [◀](#) [▶](#)
- [◀](#) [▶](#)
- [Back](#) [Close](#)
- [Full Screen / Esc](#)

- [Printer-friendly Version](#)
- [Interactive Discussion](#)



SAO OMI H₂CO retrieval

G. González Abad et al.

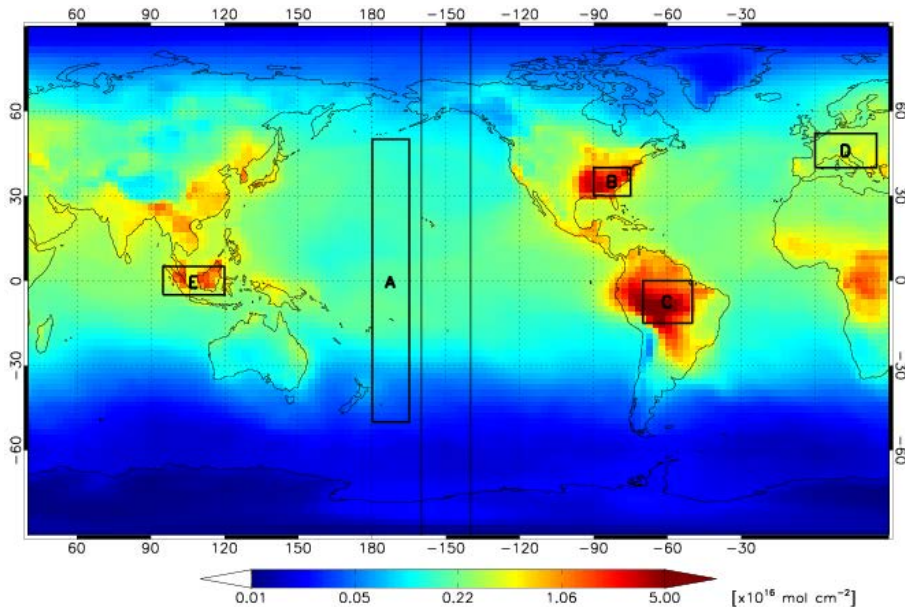


Fig. 4. August 2007 GEOS-Chem monthly mean climatology used in the calculation of the reference sector background concentrations. The portion of the remote Pacific Ocean used is enclosed by the two black vertical lines. The region above Hawaii has been excluded from the longitudinally-averaged concentrations. Note the logarithmic scale used for the colorbar. Overplotted are the 5 regions used in the time series shown in Fig. 8 as described in the text.

- [Title Page](#)
- [Abstract](#) [Introduction](#)
- [Conclusions](#) [References](#)
- [Tables](#) [Figures](#)
- [◀](#) [▶](#)
- [◀](#) [▶](#)
- [Back](#) [Close](#)
- [Full Screen / Esc](#)
- [Printer-friendly Version](#)
- [Interactive Discussion](#)



SAO OMI H₂CO retrieval

G. González Abad et al.

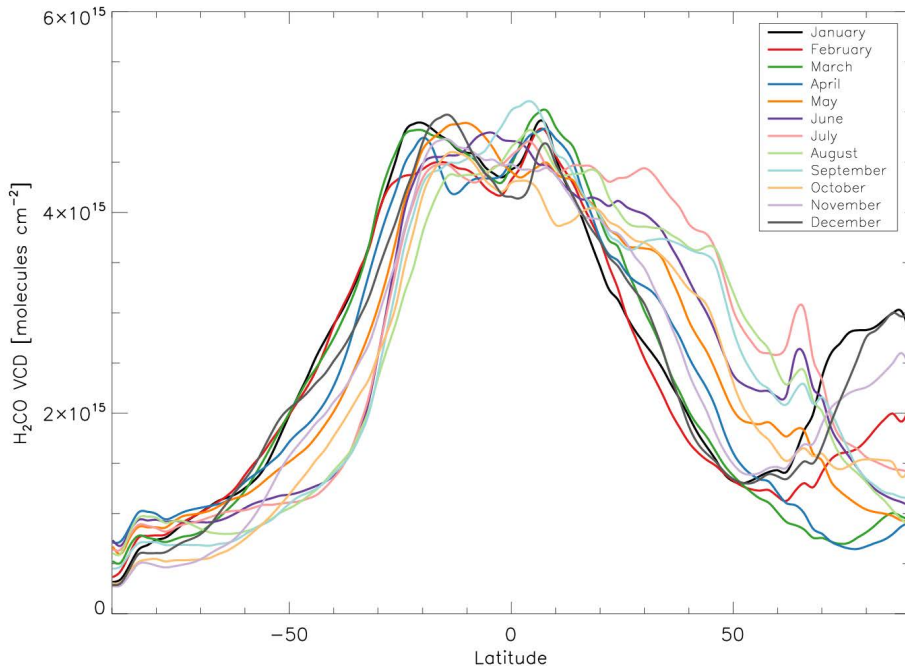


Fig. 5. Monthly reference sector longitudinally-averaged vertical column concentrations. There is a substantial monthly variability for northern latitudes, especially in winter months when unfortunately OMI is not able to measure high quality H₂CO due to the lack of light (high solar zenith angles).

- [Title Page](#)
- [Abstract](#) [Introduction](#)
- [Conclusions](#) [References](#)
- [Tables](#) [Figures](#)
- [◀](#) [▶](#)
- [◀](#) [▶](#)
- [Back](#) [Close](#)
- [Full Screen / Esc](#)
- [Printer-friendly Version](#)
- [Interactive Discussion](#)

SAO OMI H₂CO retrieval

G. González Abad et al.

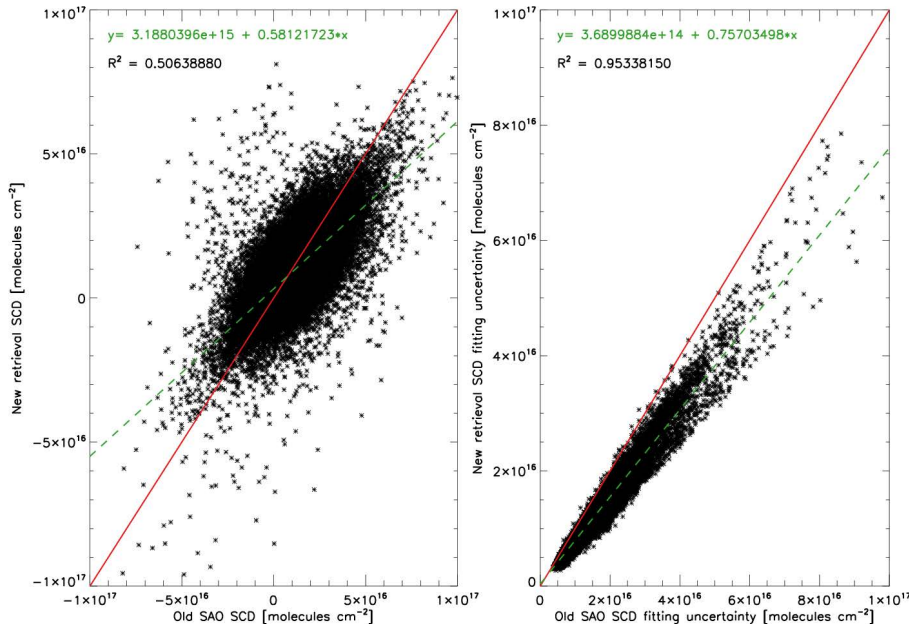


Fig. 6. Scattering plots for Orbit 43214 comparing the old SAO retrieval and new SAO retrieval of SCDs and SCDs fitting uncertainties.

- [Title Page](#)
- [Abstract](#) [Introduction](#)
- [Conclusions](#) [References](#)
- [Tables](#) [Figures](#)
- [◀](#) [▶](#)
- [◀](#) [▶](#)
- [Back](#) [Close](#)
- [Full Screen / Esc](#)
- [Printer-friendly Version](#)
- [Interactive Discussion](#)



SAO OMI H₂CO retrieval

G. González Abad et al.

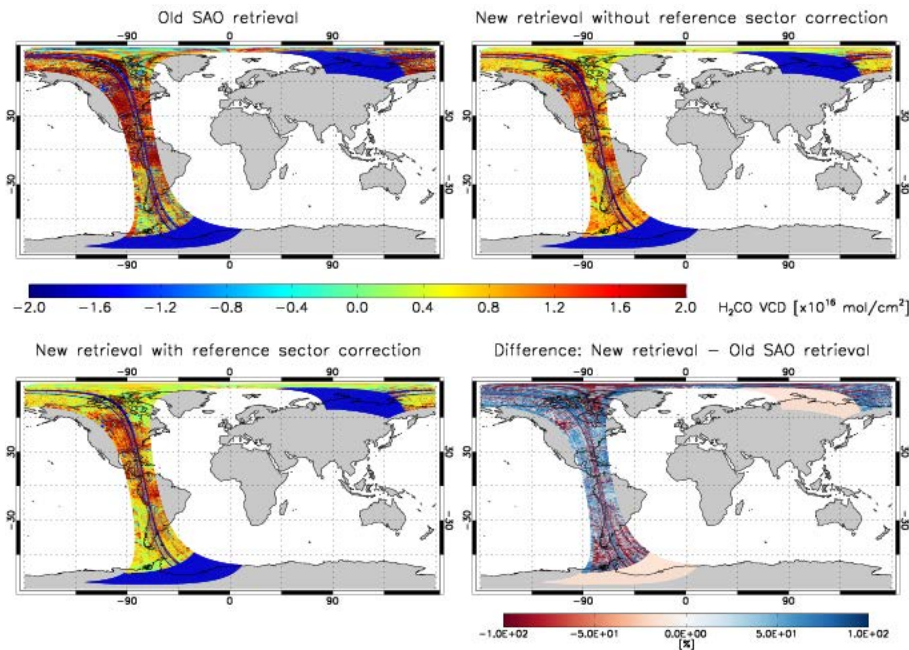


Fig. 7. VCDs retrieval for Orbit number 43214, on 29 August 2012. The panels show the old SAO retrieval (top left), the new retrieval without reference sector correction applied to it (top right), the new retrieval with the reference sector correction applied (bottom left) and the difference between the old and new retrieval with the reference sector correction applied to it expressed as % of the old operational retrieval (bottom right).

[Title Page](#)

[Abstract](#)

[Introduction](#)

[Conclusions](#)

[References](#)

[Tables](#)

[Figures](#)

[|◀](#)

[▶|](#)

[◀](#)

[▶](#)

[Back](#)

[Close](#)

[Full Screen / Esc](#)

[Printer-friendly Version](#)

[Interactive Discussion](#)



SAO OMI H_2CO retrieval

G. González Abad et al.

[Title Page](#)

[Abstract](#)

[Introduction](#)

[Conclusions](#)

[References](#)

[Tables](#)

[Figures](#)

◀

▶

◀

▶

[Back](#)

[Close](#)

[Full Screen / Esc](#)

[Printer-friendly Version](#)

[Interactive Discussion](#)

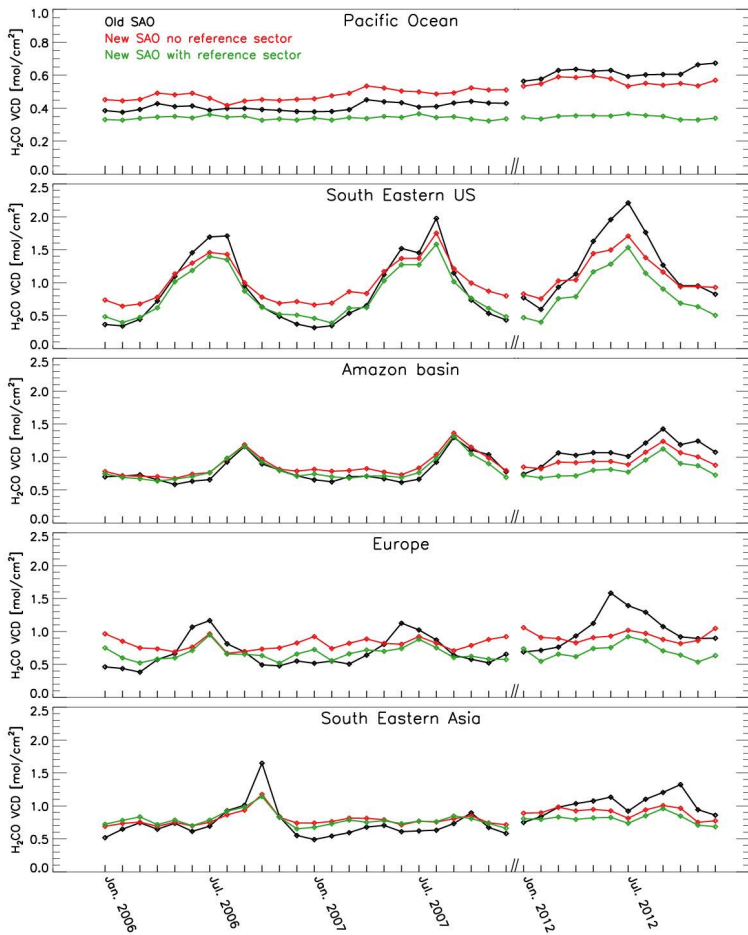


Fig. 8. Year 2006, 2007 and 2012 averaged VCDs time series for the regions depicted in Fig. 4. The break in the x axis indicates the transition from 2007 to 2012.

SAO OMI H₂CO retrieval

G. González Abad et al.

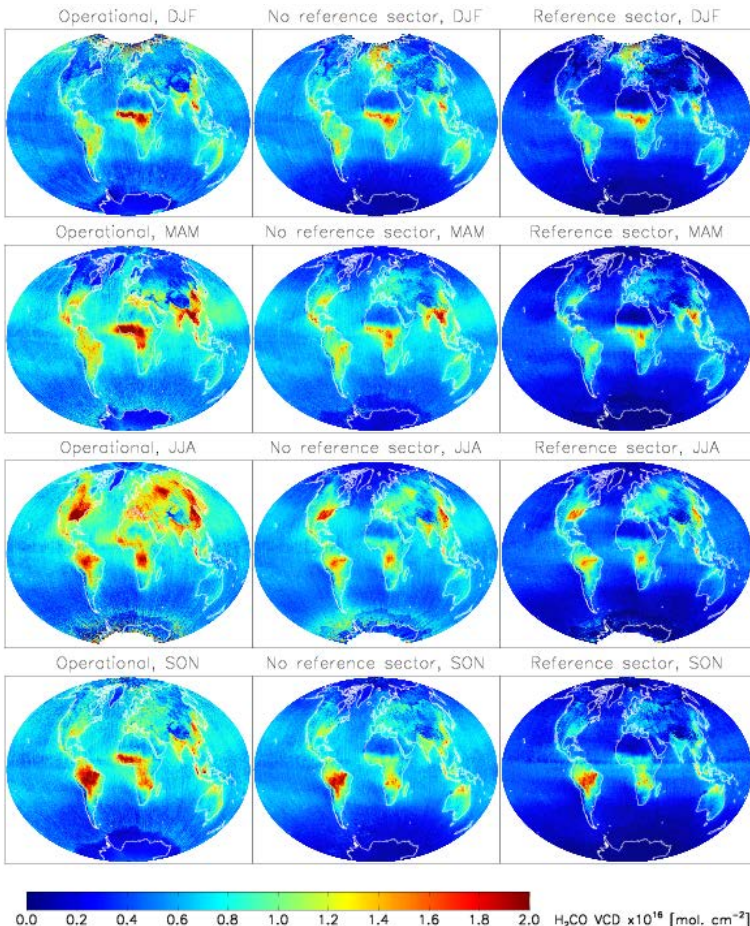


Fig. 9. Seasonal averages for 2012. Left column shows the old SAO retrieval, middle column shows the new retrieval without the reference sector correction, and right column shows new retrieval with the reference sector correction.

[Title Page](#)[Abstract](#)[Introduction](#)[Conclusions](#)[References](#)[Tables](#)[Figures](#)[|◀](#)[▶|](#)[◀](#)[▶](#)[Back](#)[Close](#)[Full Screen / Esc](#)[Printer-friendly Version](#)[Interactive Discussion](#)